When Sparsity Meets Contrastive Models: *Less* Graph Data Can Bring *Better* Class-Balanced Representations

Chunhui Zhang [1] **Chao Huang** [2] **Yijun Tian** [3] **Qianlong Wen** [3]
Zhongyu Ouyang [3] **Youhuan Li** [4] **Yanfang Ye** [3] **Chuxu Zhang** [1]

Abstract

Graph Neural Networks (GNNs) are powerful models for non-Euclidean data, but their training is often accentuated by massive unnecessary computation: On the one hand, training on non-Euclidean data has relatively high computational cost due to its irregular density properties; on the other hand, the class imbalance property often associated with non-Euclidean data cannot be alleviated by the massiveness of the data, thus hindering the generalisation of the models. To address the above issues, theoretically, we start with a hypothesis about the effectiveness of using a subset of training data for GNNs, which is guaranteed by the gradient distance between the subset and the full set. Empirically, we also observe that a subset of the data can provide informative gradients for model optimization and which changes over time dynamically. We name this phenomenon dynamic data sparsity. Additionally, we find that pruned sparse contrastive models may *"miss"* valuable information, leading to a large loss value on the informative subset. Motivated by the above findings, we develop a unified data model dynamic sparsity framework called **Data Dec**antation (DataDec) to address the above challenges. The key idea of DataDec is to identify the informative subset dynamically during the training process by applying sparse graph contrastive learning. The effectiveness of DataDec is comprehensively evaluated on graph benchmark datasets and we also verify its generalizability on image data.

[1]Brandeis University [2]University of Hong Kong [3]University of Notre Dame [4]Hunan University. Correspondence to: Chuxu Zhang <chuxuzhang@brandeis.edu>.

Proceedings of the 40^{th} International Conference on Machine Learning, Honolulu, Hawaii, USA. PMLR 202, 2023.

1. Introduction

Non-Euclidean structured data extensively exists in a wide range of applicable domains, and a considerable amount of them are naturally abstracted into graphs (e.g., social networks, biochemical molecules, etc). Such extensiveness further calls for the development of graph representation learning (GRL). Graph neural networks (GNNs) (Kipf & Welling, 2017; Hamilton et al., 2017; Veličković et al., 2018; Zhang et al., 2019; Fan et al., 2022), as the current state-of-the-art of GRL, have become essential in various graph mining applications.

However, in many real-world scenarios, the training of deep models, including GNNs often encounters two difficulties: *class imbalance* (Park et al., 2022; Ma et al., 2023) and *massive data usage* (Thakoor et al., 2021; Hu et al., 2020). First, class imbalance naturally exists in datasets from diverse practical domains. Deep models are sensitive to this property and can be biased toward the dominant classes. This bias may mislead the models' learning process, resulting in underfitting samples that are critical to the downstream tasks, and poor test performance at last. Second, the massive data required to train the model brings about heavy computation burdens, some of which are redundant regarding learning the task-related embeddings. For example, message-passing over high-degree nodes in graphs introduces the redundancy when only a few neighbors are informative. Unlike regular data such as images or texts, the connectivity of irregular data invokes random memory access, which further slows down the efficiency of data readout.

Accordingly, recent studies (Chen et al., 2021; Zhao et al., 2021; Park et al., 2022; Qian et al., 2022) arise to address the issues of *class imbalance* or *massive data usage* specifically for graphs: *(i)* On one hand, to deal with the *class imbalance* issue in node classification, Gr-aphSMOTE (Zhao et al., 2021) tries to generate new nodes for the minority classes to balance the training data. Improved upon GraphSMOTE, GraphENS (Park et al., 2022) further proposes a new augmentation method by constructing an ego network to learn the representations of the minority classes. *(ii)* On the other hand, to alleviate the *massive data usage*, (Eden et al., 2018; Chen et al., 2018) explore efficient data sampling policies

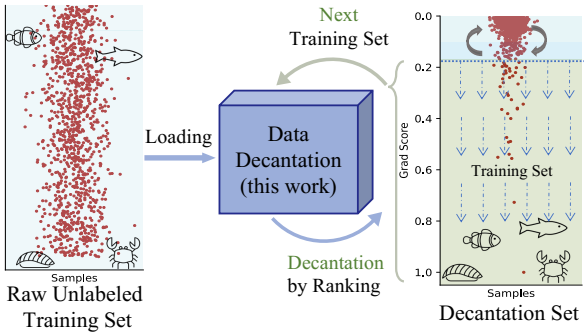

Figure 1: The principle of data decantation. It decants data samples based on rankings of their gradient scores, and then uses them as the training set in the next epoch.

to reduce the computational cost from the data perspective. From the model improvement perspective, some approaches design the quantization-aware training and low-precision inference method to reduce GNNs' operating costs on data. For example, GLT (Chen et al., 2021) applies the lottery ticket pruning technique (Frankle & Carbin, 2019) to simplify the graphs and the model concurrently.

Despite progress made so far, existing methods fail to address the class imbalance and computational burden altogether. Dealing with one may even exacerbate the condition of the other: when tackling the data imbalance, the newly synthetic nodes in GraphSMOTE and GraphENS bring along extra computational burdens for the next-coming training process. While a compact model reduces the computational burden to some extent, we interestingly found that the pruned model easily "forgets" the minorities in class-imbalanced data, reflected in its worse performance than the original model's. To investigate this observation and for further generalization, we study how each training sample affects the model's training by taking a closer look at the gradients each of them exerts. Specifically, *(i)* in the early phases of training, we identify a small subset that provides the most informative supervisory signals, as measured by the gradient norms' magnitudes (shown in later Figure 5); *(ii)* the informative subset evolves dynamically as the training process proceeds (as depicted in later Figure 3). Both the phenomenons prompt the hypothesize that *the full training set*'s training effectiveness can be approximated, to some extent, by that of the dynamic *subset*. We further show that the effectiveness of the approximation is guaranteed by the distance between the gradients of *the subset* and *the full training set*, as stated in Theorem 1.

Based on the above, we propose a general optimization framework called **Data Dec**antation (DataDec) to guide dynamic sparsity training from both the model and data aspects. The principle behind DataDec is shown in Figure 1. Since the disadvantaged but informative samples tend to bring about higher gradient magnitudes, DataDec relies on the gradients directed by dynamic sparse graph contrastive learning loss to identify the informative subsets that approximate the full set's training effectiveness. This mechanism not only does not require supervised labels, but also allows for the training of the primary model, and the pruning of the sparse one. Specifically, for each epoch, our proposed framework scores samples from the current training set and keep only k most informative samples for the next epoch. Additionally, the framework incorporates a data recycling process, which randomly recycles prior discarded samples (i.e., samples that are considered unimportant in the previous training epochs) by re-involving them in the current training process. As a result, the dynamically updated subset *(i)* supports the sparse model to learn relatively unbiased representations and *(ii)* approximates the full training set through the lens of Theorem 1. To summarize, our contributions are:

- We develop a general framework, Data Decantation which leverages dynamic sparse graph contrastive learning on class-imbalanced data for efficient data usage. To our best knowledge, this is the first study to explore the dynamic sparsity property for class-imbalanced graphs.
- We introduce cosine annealing to dynamically control the sizes of the sparse model and the data subset to smooth the training process. Meanwhile, we introduce data recycling to refresh the current data subset and avoid overfitting.
- We conduct comprehensive experiments, primarily on multiple graph benchmark datasets for the graph and node classification tasks to demonstrate DataDec's effectiveness. We further verify DataDec's generalizability to the image classification task on the CIFAR-10 dataset. Results show that DataDec outperforms the corresponding state-of-the-art methods, and its efficiency in finding the informative subset across the training epochs.

2. Related Work

Training deep model with sparsity. Parameter pruning aiming at decreasing computational cost has been a popular topic and many parameter-pruning strategies are proposed to balance the trade-off between model performance and learning efficiency (Deng et al., 2020; Liu et al., 2019). Some of them belong to the static pruning category and deep neural networks are pruned either by neurons (Han et al., 2015b; 2016) or architectures (layer and filter) (He et al., 2017; Dong et al., 2017). In contrast, recent works propose dynamic weight training strategies where different compact subnets will be dynamically activated at each training iteration (Mocanu et al., 2018; Mostafa & Wang, 2019; Raihan & Aamodt, 2020; Evci et al., 2020; Liu et al., 2023). The other line of computation cost reduction lies in the dataset sparsity (Karnin & Liberty, 2019; Mirzasoleiman et al., 2020; Paul et al., 2021; Killamsetty et al., 2021). Recently, the property of sparsity is also used to improve model

robustness (Chen et al., 2022; Fu et al., 2021; Zhang et al., 2023). In this work, we attempt to accomplish dynamic sparsity from both the GNN model and the graph dataset simultaneously.

Class-imbalanced learning on graphs. Excepting conventional node re-balanced methods, like reweighting samples (Zhao et al., 2021; Park et al., 2022) and oversampling (Zhao et al., 2021; Park et al., 2022), an early work (Zhou et al., 2018) characterizes rare classes through a curriculum strategy, while other previous works (Shi et al., 2020; Zhao et al., 2021; Park et al., 2022) tackles the class-imbalanced issue by generating synthetic samples to re-balance the dataset. Compared to the node-level task, graph-level re-balancing is under-explored. A recent work (Wang et al., 2022) proposes to use neighboring signals to alleviate graph-level class-imbalance. To the best of our knowledge, our DataDec is the first work to solve the class-imbalanced for both the node-level and graph-level tasks.

3. Methodology

In this section, we first theoretically illustrate our sparse subset approximation hypothesis, which guides the design of DataDec to continuously refine the compact training subset, especially illustrating on graphs, via the dynamic contrastive learning. The presentation is organized by the importance ranking procedure, refine smoothing, and overfitting regularization. Relevant preliminaries of GNNs, graph contrastive learning, and pruning are provided in Appendix B.

3.1. Sparse Subset Approximation Hypothesis

We first introduce the key notations used in the method. Specifically, we denote the full dataset as $\mathcal{D}_F$, the data subset used to train the model as $\mathcal{D}_S$, the learning rate as α, and the graph learning model parameters as θ (the optimal model parameters as θ*). Meanwhile, we add a superscript to represent *the data subset at epoch* t and *the model parameters trained by data subset*, i.e., $\mathcal{D}_S^{(t)}$ and $\theta^{(t)}$. Besides, we use $\mathcal{L}_{\mathcal{D}_S^{(t)};\theta^{(t)}}$ to indicate the loss of model $\theta^{(t)}$ over the dataset $\mathcal{D}_S^{(t)}$. Thus, the gradient error at the training epoch t can be computed as $\text{Err}^{(t)} = \left\|\nabla_{\theta^{(t)}}\mathcal{L}_{\mathcal{D}_S^{(t)};\theta^{(t)}} - \nabla_{\theta^{(t)}}\mathcal{L}_{\mathcal{D}_F;\theta^{(t)}}\right\|$. The sparse subset approximation hypothesis states that the model effectiveness trained on $\mathcal{D}$ can be approximated by the one trained on $\mathcal{D}_S$. Before introduce the hypothesis, we make the following mild assumption:

Assumption 1. *The model's parameters at epoch t satisfies $\left\|\theta^{(t)}\right\|^2 \leqslant d^2$, where d is a constant.*

Assumption 2. *The loss function $\mathcal{L}(\cdot)$ is convex.*

These assumptions align with previous theoretical papers on GNNs (Chen et al., 2023) or on the subset training of general machine learning (Mirzasoleiman et al., 2020; Killamsetty et al., 2021), which have also followed this philosophy to study the properties of GNNs or analyze subset training in neural networks. Inspired by these prior works and based on these assumptions, we can establish the following theorem:

Theorem 1. *Consider any model and loss function that satisfy Assumption 1 and Assumption 2, respectively. If the training loss $\mathcal{L}_{\mathcal{D}_S}$ is Lipschitz continuous, $\nabla_{\theta^{(t)}}\mathcal{L}_{\mathcal{D}_S}$ is upper-bounded by σ, and $\alpha = \frac{d}{\sigma\sqrt{T}}$, then*

$$\min_t(\mathcal{L}_{\mathcal{D}_F;\theta^{(t)}} - \mathcal{L}_{\theta*}) \leqslant \frac{d\sigma}{\sqrt{T}} + \sum_{t=1}^{T-1}\frac{d}{T}\text{Err}^{(t)}. \quad (1)$$

The detailed proof of Theorem 1 is provided in Appendix A. According to Theorem 1, it is straightforward that we can minimize the margin between the model ($\theta^{(t)}$)'s performance trained on the data subset (evaluated on $\mathcal{D}_F$) and optimal model (θ*), i.e., $\mathcal{L}_{\mathcal{D}_F;\theta^{(t)}} - \mathcal{L}_{\theta*}$, by reducing the distance between the gradients of the full dataset and the subset, i.e., $\text{Err}^{(t)}$. In other words, the optimized graph subset $\mathcal{D}_S^{(t)}$ is expected to approximate the gradients of the full dataset, and thereby exerts minimal affects on parameters' update. In contrast to DataDec, data diet (Paul et al., 2021) is designed to identify the most influential data samples $\mathcal{D}_S$ (those with largest gradients during the training phase) only at the early training stage and have them involved in further training processes, while excluding samples from $\bar{\mathcal{D}}_S = \mathcal{D}_F - \mathcal{D}_S$ with smaller gradients (i.e., $\nabla_{\theta^{(t)}}\mathcal{L}_{\mathcal{D}_S^{(t)};\theta^{(t)}} \gg \nabla_{\theta^{(t)}}\mathcal{L}_{\bar{\mathcal{D}}_S^{(t)};\theta^{(t)}}$) eternally. This one-shot selection, however, as we will show in Experiment 4.6, does not always capture the most important samples across all epochs during the training. Specifically, the rankings of elements within a specific $\mathcal{D}_S$ might be relatively static, but those within the full dataset, i.e., $\mathcal{D}_F$, are usually more dynamic, which implies the gradients of the one-shot subset $\nabla_{\theta^{(t)}}\mathcal{L}_{\mathcal{D}_S^{(t)};\theta^{(t)}}$ is unable to constantly approximate that of the full dataset $\nabla_{\theta^{(t)}}\mathcal{L}_{\mathcal{D}_F;\theta^{(t)}}$ during training.

3.2. Data Decantation

Inspired by Theorem 1 and motivated by solving the massive data usage in class-imbalanced graphs, we propose DataDec for achieving competitive performance as well as efficient data usage simultaneously by dynamically filtering out the most influential data subset. The overall framework of DataDec is illustrated in Figure 2. The training processes are summarized into four steps: (i) First, compute the gradients of the samples in $\mathcal{D}_S^{(t)}$ with respect to the contrastive learning loss; (ii) Normalize the gradients and rank the corresponding data samples in a descending order based on their gradient magnitudes; (iii) Decay the number of samples from $|\mathcal{D}_S^{(t)}|$ to $|\mathcal{D}_S^{(t+1)}|$ with cosine annealing, where we only keep the top $(1-\epsilon)|\mathcal{D}_S^{(t+1)}|$ samples (ϵ is the exploration rate which controls the ratio of the randomly

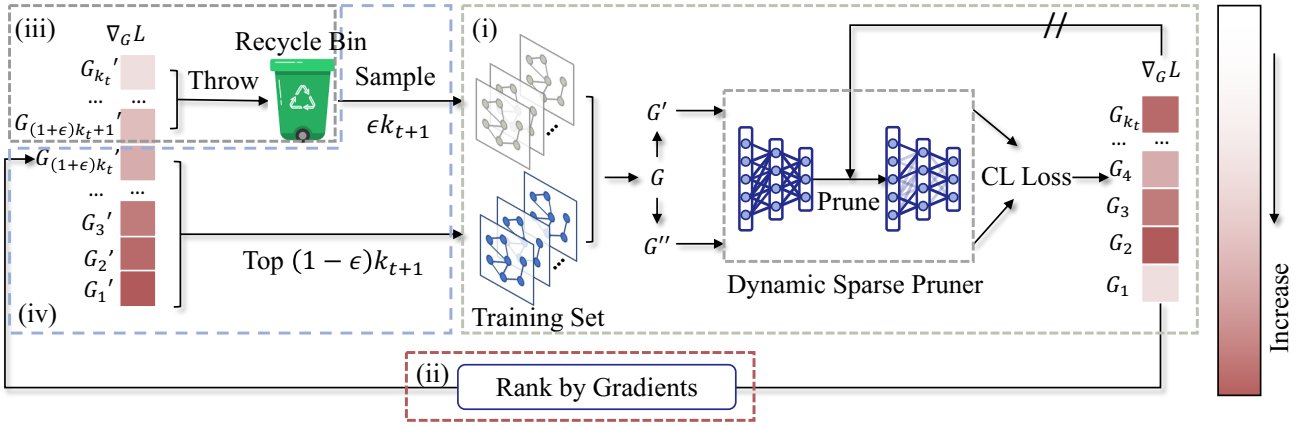

Figure 2: The overall framework of DataDec on graphs: (i) The dynamic sparse graph contrastive learning model computes gradients for data samples; (ii) The input samples are sorted according to their gradients; (iii) Part of the samples with the smallest gradients are thrown into the recycling bin; (iv) Part of the samples with the largest gradients in the current epoch and some sampled randomly from the recycling bin are jointly used as training input in the next epoch.

re-sampled samples from the recycle bin. The rest samples will hold in the recycle bin temporarily; (iv) Finally, randomly re-sample $\epsilon|\mathcal{D}_S^{(t+1)}|$ samples from the recycled bin. The union of these samples and the ones selected in step (iii) will be used for model training in the $(t+1)$-th epoch. Each of the four steps is described in detail in the following.

Compute gradients by dynamic sparse contrastive learning model. We adopt the mechanism of dynamic sparse contrastive learning in computing the gradients. The reason is two-folded: (a) it scores the samples without the supervision of any label; (b) this pruning process is more sensitive in selecting informative samples, verified in Appendix D. We omit the superscript (t) for the dataset and model parameters for simplicity in the explanation of this step. Specifically for graphs, given a graph training set $\mathcal{D} = \{G_i\}_{i=1}^N$ as input, for each training sample G_i, we randomly generate two augmented graph views, G_i' and G_i'', and feed them into the original GCN model $f_\theta(\cdot)$, and the sparse model $f_{\theta_p}(\cdot)$ pruned dynamically by the dynamic sparse pruner, respectively. The gradients are computed based on the outputs of the two GNN branches, directed by the contrastive learning loss signals. To obtain the pruned GNN, the pruner only keeps neural connections with the top-k largest weight magnitudes. Specifically, the pruned parameters of l-th GNN layer (i.e., θ^l) are selected following the formula below:

$$\theta_p^l = \text{TopK}(\theta^l, k); k = \beta^{(t)} \times |\theta^l|, \tag{2}$$

where $\text{TopK}(\theta^l, k)$ refers to the operation of selecting the top-k largest elements of θ^l, and $\beta^{(t)}$ is the fraction of the remaining neural connections, controlled by the cosine annealing formulated as follows:

$$\beta^{(t)} = \frac{\beta^{(0)}}{2}\left\{1 + \cos(\frac{\pi t}{T})\right\}, t \in [1, T], \tag{3}$$

where $\beta^{(0)}$ is initialized as 1. In addition, we refresh θ_p^l every few epochs to reactivate neurons based on their gradients, following the formula below:

$$\mathbb{I}_{\theta_g^l} = \text{argTopK}(\nabla_{\theta^l}\mathcal{L}_{\mathcal{D}_S;\theta}, k); k = \beta^{(t)} \times |\theta^l|, \tag{4}$$

where argTopK returns the indices of the top-k largest elements $\mathbb{I}_{\theta_g^l}$ of the corresponding neurons θ_g^l. To further elaborate, we refresh θ_p^l every few epochs by $\theta_p^l \leftarrow \theta_p^l \cup \theta_g^l$, as the updated pruned parameters to be involved in the next iteration. After we obtain the pruned model, gradients are computed based on the contrastive learning loss between $f_\theta(G_i')$ and $f_{\theta_p}(G_i'')$, which are then saved for the further ranking process. For other data such as images, corresponding augmenters and backbones are chosen to adapt to the DataDec framwork.

Rank samples according to their gradients' L_2 norms. In order to find the relative importance of the samples, we rank the samples based on the gradients each of them brings about, saved in the previous training epoch by the last step. Specifically, at each of the t-th training epoch, we score each sample by the L_2 norm of its gradient:

$$g(G_i) = \left\|\nabla_\theta \mathcal{L}\left(f_\theta(G_i'), f_{\theta_p}(G_i'')\right)\right\|_2, \tag{5}$$

where $\mathcal{L}$ is the popular InfoNCE (Van den Oord et al., 2018) loss in contrastive learning, taking the outputs of the two model branches as inputs. Therefore, the gradient is calculated as follows:

$$\nabla_\theta \mathcal{L}(f_\theta(G_i'), f_{\theta_p}(G_i'')) = p_\theta(G') - p_{\theta_p}(G_i''), \tag{6}$$

where $p_\theta(G_i')$ and $p_{\theta_p}(G_i'')$ are the normalized model's predictions, i.e., $p(\cdot) = S(f(\cdot))$ and $S(\cdot)$ is the softmax function or sigmoid function. The samples are ranked by the values calculated by Eq. 5.

Decay the size of $\mathcal{D}_S$ by cosine annealing. For decreasing the size of the subset, we use cosine annealing when the training process proceeds. As we will show in Figure 3 for the experiments, some graph samples showing low scores of importance at the early training stage may be highly-scored again if given more patience in the later training epochs. Therefore, chunking the size of the sparse subset radically in one shot deprives the chances of the potential samples informing the models at a later stage. To tackle this issue, we employ cosine annealing to gradually decrease the size of the subset:

$$|\mathcal{D}_S^{(t)}| = \frac{|\mathcal{D}|}{2}\left\{1+\cos(\frac{\pi(t)}{T})\right\}, t \in [1, T]\,. \tag{7}$$

Note that this process not only automatically decreases the size of $\mathcal{D}_S$ smoothly, but also avoids the manual one-shot selection as in the data diet (Paul et al., 2021).

Recycle removed samples for the next training epoch. We aim to update the elements in $\mathcal{D}_S^{(t)}$ obtained in the last step. Since current low-scored samples may still have the potential to be highly-scored in the later training epochs, we randomly recycle a proportion of the removed samples and re-involve them in the training process again. Specifically, the exploration rate ϵ controls the proportion of data that substitutes a number of $\epsilon|\mathcal{D}_S^{t+1}|$ samples with the lowest scores with the same amount of randomly selected samples in $\mathcal{D}_S^{(t+1)}$. At the t-th epoch, the update rule is formulated as follows:

$$\begin{aligned}\mathcal{D}S^{(t+1)} = &\ \mathrm{TopK}(\mathcal{D}S^{(t)}, (1-\epsilon)|\mathcal{D}S^{(t+1)}|) \\ &\bigcup \mathrm{SampleK}(\bar{\mathcal{D}S}^{(t-1)}, \epsilon|\mathcal{D}_S^{(t+1)}|),\end{aligned} \tag{8}$$

where $\mathrm{SampleK}(\bar{\mathcal{D}_S}^{(t-1)}, \epsilon|\mathcal{D}_S^{(t+1)}|)$ returns randomly sampled $\epsilon|\mathcal{D}_S^{(t+1)}|$ samples from $\bar{\mathcal{D}_S}^{(t-1)}$, saved in the last epoch. We utilize the compact sparse subset $\mathcal{D}_S^{(t+1)}$ for the training purposes at $(t+1)$-th epoch, and repeat the previous pipelines until T epochs.

4. Experiments

In this section, we conduct extensive experiments to validate the effectiveness and generalization ability of our proposed model for both the graph and node classification tasks on imbalanced graph datasets, as well as the image classification task on CIFAR-10. We also conduct an ablation study and informative subset evolution analysis to further prove the effectiveness. Due to space limitations, more analysis validating DataDec's properties and resource cost are provided in Appendix D and E.

4.1. Experimental Setup

Datasets. To validate the effectiveness of our model, we primarily validate it on various graph benchmark datasets for the two classification tasks under the class-imbalanced data scenario. For the class-imbalanced graph classification task, we choose the seven validation datasets in the G^2GNN paper (Wang et al., 2022): MUTAG, PROTEINS, D&D, NCI1, PTC-MR, DHFR, and REDDIT-B (Morris et al., 2020). For the class-imbalanced node classification task, we choose the five datasets in the GraphENS paper (Park et al., 2022): Cora-LT, CiteSeer-LT, PubMed-LT (Sen et al., 2008), Amazon-Photo, and Amazon-Computers. We extend the list with CIFAR-10 (Krizhevsky et al., 2009), a classic image dataset, to verify the generalization ability of DataDec. Detailed descriptions of these datasets are provided in Appendix C.1.

Baselines. We compare our model with a variety of baseline methods with different rebalancing methods. For the class-imbalanced graph classification, we consider three rebalancing methods: vanilla (without rebalancing when training), up-sampling (Wang et al., 2022), and re-weighting (Wang et al., 2022). For each rebalancing method, we run three baseline methods including GIN (Xu et al., 2019), InfoGraph (Sun et al., 2019), and GraphCL (You et al., 2020). In addition, we adopt two versions of G^2GNN (remove-edge and mask-node)(Wang et al., 2022) for in-depth comparison. For the class-imbalanced node classification, we consider nine baseline methods including vanilla, SynFlow(Tanaka et al., 2020), BGRL (Thakoor et al., 2021), GRACE (Zhu et al., 2020), re-weighting (Japkowicz & Stephen, 2002), oversampling (Park et al., 2022), cRT (Kang et al., 2020), PC Softmax (Hong et al., 2021), DR-GCN (Shi et al., 2020), GraphSMOTE (Zhao et al., 2021), and GraphENS (Park et al., 2022). For the image classification task on CIFAR-10, we choose Forget Score (Toneva et al., 2019) and Data Diet (EL2N-based and GradNd-based) (Paul et al., 2021) for comparison. Further details about the baselines are illustrated in Appendix C.2.

Evaluation Metrics. To evaluate the model performance, we use the F1-micro (F1-mi.) and F1-macro (F1-ma.) scores as the metrics for the class-imbalanced graph classification task, and accuracy (Acc.), balanced accuracy (bAcc.), and F1-macro (F1-ma.) score for the node classification task.

Experimental Settings. For graph tasks, we use GCN (Kipf & Welling, 2017) as the GNN backbone in DataDec. Specifically, we concatenate a two-layer GCN with a one-layer fully-connected layer for node classification, and add an additional average pooling layer for graph classification. We follow the settings in (Wang et al., 2022) and (Park et al., 2022) to vary the imbalance ratios for graph and node classification tasks, respectively. In addition, we employ GraphCL (You et al., 2020) as the graph contrastive learning

Table 1: Class-imbalanced graph classification results. Numbers after each dataset name indicate imbalance ratios of minority to majority categories. Best/second-best results are in bold/underline. The results with standard deviations, and additional datasets PTC-MR, DHFR, REDDIT-B, and their average ranks are provided in Table 6, Appendix C.4.

Rebalance Method	Basis	MUTAG (5:45)		PROTEINS (30:270)		D&D (30:270)		NCI1 (100:900)		Sparsity (%)	
		F1-ma.	F1-mi.	F1-ma.	F1-mi.	F1-ma.	F1-mi.	F1-ma.	F1-mi.	data	model
vanilla	GIN	52.50	56.77	25.33	28.50	9.99	11.88	18.24	18.94	100	100
	InfoGraph	69.11	69.68	35.91	36.81	21.41	27.68	33.09	34.03	100	100
	GraphCL	66.82	67.77	40.86	41.24	21.02	26.80	31.02	31.62	100	100
up-sampling	GIN	78.03	78.77	65.64	71.55	41.15	70.56	59.19	71.80	>100	100
	InfoGraph	78.62	79.09	62.68	66.02	41.55	71.34	53.38	62.20	>100	100
	GraphCL	80.06	80.45	64.21	65.76	38.96	64.23	49.92	58.29	>100	100
re-weight	GIN	77.00	77.68	54.54	55.77	28.49	40.79	36.84	39.19	100	100
	InfoGraph	80.85	81.68	65.73	69.60	41.92	72.43	53.05	62.45	100	100
	GraphCL	80.20	80.84	63.46	64.97	40.29	67.96	50.05	58.18	100	100
G^2GNN	remove edge	80.37	81.25	<u>67.70</u>	73.10	43.25	<u>77.03</u>	63.60	72.97	100	100
	mask node	<u>83.01</u>	<u>83.59</u>	67.39	<u>73.30</u>	<u>43.93</u>	**79.03**	<u>64.78</u>	<u>74.91</u>	100	100
DataDec (ours)	dynamic sparsity	**85.71**	**85.71**	**68.32**	**75.84**	**44.01**	<u>77.02</u>	**65.73**	**76.02**	50	50

framework, and use cosine annealing to dynamically control the sparsity rate in the GNN model and the dataset. For the CIFAR-10 image classification task, we adopt ResNet18 (He et al., 2016) as the backbone model and follow the other settings in Data Diet (Paul et al., 2021). The target pruning ratio for the model is set to 0.75, and the pruning ratio for the dataset is set to 1.0. After contrastive pre-training, we use the model's output logits as input to a Support Vector Machine (SVM) for fine-tuning. DataDec is implemented in PyTorch and trained on an NVIDIA V100 GPU.

4.2. Class-imbalanced Graph Classification

The evaluated results for the graph classification task on class-imbalanced graph datasets are reported in Table 1, with the best performance and runner-ups shown in bold and underlined, respectively. From the table, it is evident that DataDec outperforms baseline methods on both metrics across different datasets, while utilizing an average of 50% data and 50% model weights per round. Although a slight difference in F1-micro has been observed between DataDec and the best baseline method G^2GNN on the D&D dataset, this can be attributed to the significantly larger size of graphs in D&D compared to other datasets, which necessitates specialized designs for graph augmentations. For example, the average graph size in terms of node number is 284.32 for D&D, but only 39.02 and 17.93 for PROTEINS and MUTAG, respectively. However, even on the same dataset, G^2GNN achieves only 43.93 on F1-macro, while DataDec reaches 44.01, showcasing DataDec's ability to learn effectively even on large graph datasets. Specifically, models trained under the vanilla setting perform the worst due to their ignorance of the class imbalance. The up-sampling strategy improves performance but introduces unnecessary data usage by sampling the minority classes multiple times. Similarly, the re-weighting strategy attempts to address the class imbalance issue by assigning different weights to different samples but requires labels for weight calculation and may not generalize well when labels are missing. G^2GNN, as the best baseline method, achieves decent performance by considering rich supervisory signals from both globally and locally neighboring graphs. Finally, the proposed model, DataDec, achieves the best performance by effectively capturing dynamic data sparsity from both the model and data perspectives. Furthermore, we rank the performance of DataDec compared to baseline methods on each dataset. DataDec achieves an average rank of 1.00 and 1.14, further demonstrating its superiority. It is worth noting that all existing methods utilize the entire datasets and model weights, whereas DataDec achieves superior performance by utilizing only half of the data and weights.

4.3. Class-imbalanced Node Classification

For the class-imbalanced node classification task, we first evaluate DataDec on three long-tailed citation graphs (Cora-LT, CiteSeer-LT, and PubMed-LT) and present the results in Table 2. We observe that DataDec achieves the best performance compared to baseline methods across different metrics. GraphSMOTE and GraphENS achieve satisfactory performance by generating virtual nodes to enhance the representation of minority classes. In contrast, DataDec does not rely on synthetic virtual nodes to learn balanced representations, thereby avoiding unnecessary computational costs. Similar to the class-imbalanced graph classification task discussed in Section 4.2, DataDec demonstrates superior performance by utilizing only half of the data and weights, whereas all baselines perform worse even with the

Table 2: Class-imbalanced node classification results. Best/second-best results are in bold/underline. The results with standard deviations are provided in Table 7, Appendix C.4.

Method	Cora-LT			CiteSeer-LT			PubMed-LT			A.P. (ρ =82)		A.C. (ρ =244)		Sparsity (%)	
	Acc.	bAcc.	F1-ma.	Acc.	bAcc.	F1-ma.	Acc.	bAcc.	F1-ma.	(b)Acc.	F1-ma.	(b)Acc.	F1-ma.	data	model
vanilla	73.66	62.72	63.70	53.90	47.32	43.00	70.76	57.56	51.88	82.86	78.72	68.47	64.01	100	100
SynFlow	72.98	60.62	63.29	52.85	46.23	42.19	69.63	56.75	50.99	81.57	76.93	68.10	62.97	100	N.A.
GRACE	74.72	63.95	65.26	54.94	50.87	46.90	72.37	63.22	58.18	83.57	83.61	73.02	64.52	100	100
BGRL	73.81	64.95	64.87	56.84	50.83	47.04	74.17	62.21	59.07	83.49	82.37	75.88	63.15	100	100
Re-Weight	75.20	68.79	69.27	62.56	55.80	53.74	77.44	72.80	73.66	92.94	92.95	90.04	90.11	100	100
Oversampling	77.44	70.73	72.40	62.78	56.01	53.99	76.70	68.49	69.50	92.46	92.47	89.79	89.85	>100	100
cRT	76.54	69.26	70.95	60.60	54.05	52.36	75.10	67.52	68.08	91.24	91.17	86.02	86.00	100	100
PC Softmax	76.42	71.30	71.24	65.70	**61.54**	61.49	76.92	75.82	74.19	93.32	93.32	86.59	86.62	100	100
DR-GCN	73.90	64.30	63.10	56.18	49.57	44.98	72.38	58.86	53.05	N/A	N/A	N/A	N/A	100	100
GraphSmote	76.76	69.31	70.21	62.58	55.94	54.09	75.98	70.96	71.85	92.65	92.61	89.31	89.39	>100	100
GraphENS	77.76	72.94	73.13	**66.92**	60.19	58.67	78.12	74.13	74.58	93.82	93.81	91.94	91.94	>100	100
DataDec (ours)	**78.29**	**73.94**	**74.25**	**66.90**	**61.56**	**61.85**	**78.20**	**76.05**	**76.32**	**93.85**	**94.02**	**92.19**	**92.16**	50	50

Table 3: Results comparison on image classification.

Strategy	Test Acc. (%)	Data Sparsity (%)
No Pruning	95.27	100
Random Pruning	93.38	50
Forget Score	95.34	50
Data Diet (EL2N)	95.21	50
Data Diet (GradNd)	95.16	50
DataDec (ours)	**95.66**	50

full dataset and weights. To validate the effectiveness of the proposed model on real-world data, we evaluate DataDec on naturally class-imbalanced benchmark datasets (Amazon-Photo and Amazon-Computers). We observe that DataDec outperforms other methods on both datasets, highlighting its effectiveness across diverse practical scenarios.

4.4. Generalizability to Image Domain

We conducted further evaluations to assess the generalization ability of DataDec on a widely used benchmark image dataset: CIFAR-10. We compared DataDec with Forget Score (Toneva et al., 2019) and Data Diet (EL2N-based and GradNd-based) (Paul et al., 2021). The results presented in Table 3 demonstrate that DataDec outperforms the previous methods. Notably, the second-best method, Forget Score, requires an additional subset selection period of 200 epochs, which is not part of the regular training phase (200 training epochs) and utilizes a significantly larger number of epochs compared to our framework. Taking into account both accuracy and training epochs, our framework showcases its promising and versatile potential for handling data from other domains.

4.5. Ablation Study

Since DataDec is a unified learning framework that relies on multiple components to employ dynamic sparsity training from both the model and dataset perspectives, we conducted an ablation study to validate the effectiveness of each component. Specifically, DataDec utilizes four components to address data sparsity and imbalance: pruning samples by ranking gradients (GS), training with a sparse dataset (SS), using cosine annealing to reduce dataset size (CAD), and recycling removed samples (RS). Additionally, it employs four components to address model sparsity and data imbalance: pruning weights by ranking magnitudes (RM), using a sparse GNN (SG), using cosine annealing to progressively reduce the size of the sparse GNN (CAG), and reactivating removed weights (RW). DataDec also incorporates self-supervision to calculate the gradient score. Detailed information on model variants can be found in Appendix C.3. We analyzed the contributions of each component by independently removing them for both tasks. The results are presented in Table 4.

From the table, we observe that the performance consistently drops after removing any component, highlighting the effectiveness of each component in the framework. Both mechanisms for addressing data and model sparsity significantly contribute to the overall performance, emphasizing the necessity of these two mechanisms in tackling sparsity-related challenges. Self-supervision plays a similar role to the dynamic sparsity by enabling the identification of informative data samples without relying on label supervision. Within the dataset dynamic sparsity mechanism, GS and CAD demonstrate the highest contributions. This indicates that the discriminability of the sparse GNN effectively identifies hidden dynamic sparse subsets in an accurate and efficient manner. Regarding the model dynamic sparsity mechanism, removing RM and SG results in a notable performance drop, emphasizing their crucial roles in training the dynamic sparse GNN from the full GNN model. CAG plays a vital role in ensuring performance stability after model pruning and aids in capturing informative samples during the decantation process by assigning higher gradient norms. Among these variants, the full model DataDec consistently achieves the best results, highlighting the importance of combining dynamic sparsity mechanisms from both perspectives and utilizing the self-supervision strategy.

Table 4: Ablation study results for both graph and node classification tasks. Four rows of red represent removing four individual components from data sparsity perspective. Four rows of blue represent removing four individual components from model sparsity perspective. Best results are in bold.

	Class-imbalanced Graph Classification (F1-ma.)							Class-imbalanced Node Classification (Acc.)				
Variant	MUTAG	PROTEINS	D&D	NCI1	PTC-MR	DHFR	REDDIT-B	Cora-LT	CiteSeer-LT	PubMed-LT	A. Photos	A. Computer
DataDec	**85.71**	**68.32**	**44.01**	**65.73**	**47.07**	62.25	**69.70**	**78.29**	**66.90**	**78.20**	**93.85**	**92.19**
w/o GS	80.10	63.42	36.61	61.80	42.12	48.57	61.40	68.96	60.33	56.22	73.22	67.84
w/o SS	80.95	63.55	42.19	62.30	45.21	61.99	70.61	77.15	64.67	76.15	79.09	91.33
w/o CAD	78.41	57.99	40.23	60.61	44.96	50.00	67.15	74.87	62.62	75.35	90.71	83.23
w/o RS	83.21	59.32	41.65	60.51	35.21	60.99	67.61	73.27	61.32	72.02	87.11	90.38
w/o RM	44.37	40.42	38.45	34.39	32.14	43.75	64.82	70.97	54.58	70.16	79.01	65.38
w/o SG	82.63	65.96	42.50	69.10	35.19	61.42	69.16	77.54	67.43	72.43	91.25	90.05
w/o CAG	83.50	54.04	40.21	51.82	34.20	62.41	64.14	75.78	63.43	73.07	92.77	87.40
w/o RW	79.25	56.33	38.34	63.00	38.00	61.53	63.16	76.46	65.36	75.54	90.54	89.10
w/o S.S.	80.07	63.90	39.77	57.22	38.60	**62.30**	65.67	74.82	65.28	74.00	86.14	86.40

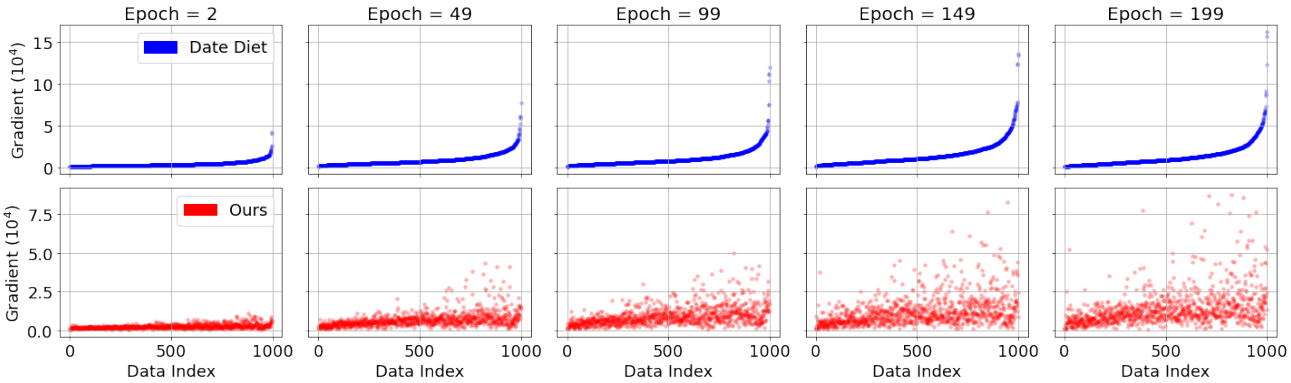

Figure 3: Evolution of data samples' gradients computed by data diet (Paul et al., 2021) (upper figures) and our DataDec (lower figures) on NCI1 dataset.

4.6. Analyzing Evolution of Sparse Subset by Scoring All Samples

To showcase the dynamic capability of DataDec in identifying informative samples, we present visualizations of the sparse subset evolution of Data Diet and DataDec on the class-imbalanced NCI1 dataset in Figure 3. In this analysis, we compute importance scores for 1000 graph samples and rank them accordingly, marking each sample with its corresponding index. The upper figures in Figure 3 demonstrate that Data Diet struggles to accurately identify dynamic informative nodes. Once a data sample is removed from the training list due to a low score, it is permanently disregarded by the model. However, it is important to note that the current lack of importance does not necessarily imply that a sample will remain unimportant indefinitely. This becomes especially evident in the early training stages when the model is unable to accurately detect the true importance of each sample, leading to premature elimination of crucial nodes. Similarly, if a data sample is deemed important during the initial epochs (indicated by a higher sample index), it cannot be removed in subsequent epochs. Consequently, we observe that Data Diet can only increase the scores of samples within a high index range (i.e., 500-1000) while ignoring samples within the low index range (i.e., < 500). In contrast, DataDec (Figure 3 bottom) excels at capturing the dynamic importance of each sample, irrespective of its initial importance score. We observe that samples with varying indexes have the opportunity to be considered important and thus included in the training list. Consequently, DataDec takes into account a broader range of data samples when shrinking the training list while maintaining flexibility regarding previous importance scores.

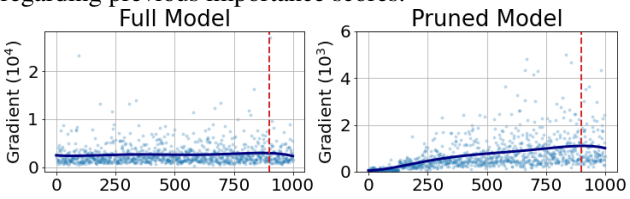

Figure 4: Results of data samples' gradients computed by full GNN model and our dynamic sparse GNN model on NCI1 data. Red dashed line: on the left side, points on the x-axis $[0, 900]$ are majority class; on the right side, points on the x-axis $[900, 1000]$ are minority class.

4.7. Finding Informative Samples by Sparse GNN

In comparison to the full GNN, our dynamic sparse GNN exhibits increased sensitivity in recognizing informative

data samples, as empirically demonstrated in Figure 4. In our dynamic pruned model, larger gradients are assigned to the minority class compared to the majority class during the contrastive training. Conversely, the full model tends to assign relatively uniform gradients to both classes. As a result, the proposed dynamically pruned model showcases its discriminatory ability specifically for the minority class. This ability within our DataDec framework proves effective in addressing the class-imbalance issue.

5. Conclusion

In this paper, we propose Data Decantation (DataDec), an efficient method to address the challenge of class imbalance in graph data. Using dynamic sparse graph contrastive learning, DataDec dynamically identifies a sparse yet informative subset for model training. Our method, which incorporates a sparse GNN encoder that is dynamically sampled from a dense GNN and then uses its sensitivity to informative sample identification to rank and update the training data subset in each epoch, outperforms state-of-the-art baselines for both node and graph classification tasks in class-imbalanced scenarios. Additionally, our analysis of the evolution of the sparse informative samples further demonstrates the superiority of DataDec in effectively identifying the informative subset throughout the training process.

Acknowledgement

This work is partially supported by the NSF under grants CMMI-2146076 and Brandeis University. Any opinions, findings, conclusions or recommendations expressed in this material are those of the authors and do not necessarily reflect the views of any funding agencies.

References

Chen, J., Ma, T., and Xiao, C. FastGCN: Fast learning with graph convolutional networks via importance sampling. In *ICLR*, 2018.

Chen, T., Sui, Y., Chen, X., Zhang, A., and Wang, Z. A unified lottery ticket hypothesis for graph neural networks. In *ICML*, 2021.

Chen, T., Zhang, Z., pengjun wang, Balachandra, S., Ma, H., Wang, Z., and Wang, Z. Sparsity winning twice: Better robust generalization from more efficient training. In *ICLR*, 2022.

Chen, Z., Li, P., Liu, H., and Hong, P. Characterizing the influence of graph elements. In *ICLR*, 2023.

Deng, L., Li, G., Han, S., Shi, L., and Xie, Y. Model compression and hardware acceleration for neural networks: A comprehensive survey. In *Proceedings of the IEEE*. IEEE, 2020.

Dong, X., Chen, S., and Pan, S. Learning to prune deep neural networks via layer-wise optimal brain surgeon. *NeurIPS*, 30, 2017.

Eden, T., Jain, S., Pinar, A., Ron, D., and Seshadhri, C. Provable and practical approximations for the degree distribution using sublinear graph samples. In *WWW*, 2018.

Evci, U., Gale, T., Menick, J., Castro, P. S., and Elsen, E. Rigging the lottery: Making all tickets winners. In *ICML*, 2020.

Fan, Y., Ju, M., Zhang, C., and Ye, Y. Heterogeneous temporal graph neural network. In *SDM*, 2022.

Fey, M. and Lenssen, J. E. Fast graph representation learning with PyTorch Geometric. In *ICLR Workshop on Representation Learning on Graphs and Manifolds*, 2019.

Frankle, J. and Carbin, M. The lottery ticket hypothesis: Finding sparse, trainable neural networks. In *ICLR*, 2019.

Fu, Y., Yu, Q., Li, M., Chandra, V., and Lin, Y. Double-win quant: Aggressively winning robustness of quantized deep neural networks via random precision training and inference. In *ICML*, 2021.

Hamilton, W. L., Ying, R., and Leskovec, J. Inductive representation learning on large graphs. In *NIPS*, 2017.

Han, S., Mao, H., and Dally, W. J. Deep compression: Compressing deep neural networks with pruning, trained quantization and huffman coding. *arXiv preprint arXiv:1510.00149*, 2015a.

Han, S., Pool, J., Tran, J., and Dally, W. Learning both weights and connections for efficient neural network. In *NeurIPS*, 2015b.

Han, S., Mao, H., and Dally, W. J. Deep compression: Compressing deep neural networks with pruning, trained quantization and huffman coding. In *ICLR*, 2016.

He, K., Zhang, X., Ren, S., and Sun, J. Deep residual learning for image recognition. In *CVPR*, 2016.

He, Y., Zhang, X., and Sun, J. Channel pruning for accelerating very deep neural networks. In *ICCV*, 2017.

Hong, Y., Han, S., Choi, K., Seo, S., Kim, B., and Chang, B. Disentangling label distribution for long-tailed visual recognition. In *CVPR*, 2021.

Hu, W., Fey, M., Zitnik, M., Dong, Y., Ren, H., Liu, B., Catasta, M., and Leskovec, J. Open graph benchmark: Datasets for machine learning on graphs. *arXiv preprint arXiv:2005.00687*, 2020.

Japkowicz, N. and Stephen, S. The class imbalance problem: A systematic study. *Intelligent Data Analysis*, 2002.

Kang, B., Xie, S., Rohrbach, M., Yan, Z., Gordo, A., Feng, J., and Kalantidis, Y. Decoupling representation and classifier for long-tailed recognition. In *ICLR*, 2020.

Karnin, Z. and Liberty, E. Discrepancy, coresets, and sketches in machine learning. In *COLT*, 2019.

Killamsetty, K., Durga, S., Ramakrishnan, G., De, A., and Iyer, R. Grad-match: Gradient matching based data subset selection for efficient deep model training. In *ICML*, 2021.

Kipf, T. N. and Welling, M. Semi-supervised classification with graph convolutional networks. In *ICLR*, 2017.

Krizhevsky, A., Hinton, G., et al. Learning multiple layers of features from tiny images. *Technical Report*, 2009.

Liu, Z., Sun, M., Zhou, T., Huang, G., and Darrell, T. Rethinking the value of network pruning. In *ICLR*, 2019.

Liu, Z., Zhang, C., Tian, Y., Zhang, E., Huang, C., Ye, Y., and Zhang, C. Fair graph representation learning via diverse mixture-of-experts. In *WWW*, 2023.

Ma, Y., Tian, Y., Moniz, N., and Chawla, N. V. Class-imbalanced learning on graphs: A survey. *arXiv preprint arXiv:2304.04300*, 2023.

Mirzasoleiman, B., Bilmes, J., and Leskovec, J. Coresets for data-efficient training of machine learning models. In *ICML*, 2020.

Mocanu, D. C., Mocanu, E., Stone, P., Nguyen, P. H., Gibescu, M., and Liotta, A. Scalable training of artificial neural networks with adaptive sparse connectivity inspired by network science. *Nature Communications*, 2018.

Morris, C., Kriege, N. M., Bause, F., Kersting, K., Mutzel, P., and Neumann, M. Tudataset: A collection of benchmark datasets for learning with graphs. In *ICML Workshop on Graph Representation Learning and Beyond*, 2020.

Mostafa, H. and Wang, X. Parameter efficient training of deep convolutional neural networks by dynamic sparse reparameterization. In *ICML*, 2019.

Oord, A. v. d., Li, Y., and Vinyals, O. Representation learning with contrastive predictive coding. *arXiv preprint arXiv:1807.03748*, 2018.

Park, J., Song, J., and Yang, E. GraphENS: Neighbor-aware ego network synthesis for class-imbalanced node classification. In *ICLR*, 2022.

Paul, M., Ganguli, S., and Dziugaite, G. K. Deep learning on a data diet: Finding important examples early in training. In *NeurIPS*, 2021.

Qian, Y., Zhang, C., Zhang, Y., Wen, Q., Ye, Y., and Zhang, C. Co-modality graph contrastive learning for imbalanced node classification. In *NeurIPS*, 2022.

Raihan, M. A. and Aamodt, T. Sparse weight activation training. *NeurIPS*, 2020.

Sen, P., Namata, G., Bilgic, M., Getoor, L., Galligher, B., and Eliassi-Rad, T. Collective classification in network data. *AI Magazine*, 2008.

Shi, M., Tang, Y., Zhu, X., Wilson, D., and Liu, J. Multi-class imbalanced graph convolutional network learning. In *IJCAI*, 2020.

Sun, F.-Y., Hoffman, J., Verma, V., and Tang, J. Infograph: Unsupervised and semi-supervised graph-level representation learning via mutual information maximization. In *ICLR*, 2019.

Tanaka, H., Kunin, D., Yamins, D. L., and Ganguli, S. Pruning neural networks without any data by iteratively conserving synaptic flow. In *NeurIPS*, 2020.

Thakoor, S., Tallec, C., Azar, M. G., Azabou, M., Dyer, E. L., Munos, R., Veličković, P., and Valko, M. Large-scale representation learning on graphs via bootstrapping. In *ICLR*, 2021.

Toneva, M., Sordoni, A., des Combes, R. T., Trischler, A., Bengio, Y., and Gordon, G. J. An empirical study of example forgetting during deep neural network learning. In *ICLR*, 2019.

Van den Oord, A., Li, Y., and Vinyals, O. Representation learning with contrastive predictive coding. *arXiv preprint arXiv:1807.03748*, 2018.

Veličković, P., Cucurull, G., Casanova, A., Romero, A., Liò, P., and Bengio, Y. Graph attention networks. In *ICLR*, 2018.

Wang, Y., Zhao, Y., Shah, N., and Derr, T. Imbalanced graph classification via graph-of-graph neural networks. In *CIKM*, 2022.

Wu, Z., Pan, S., Chen, F., Long, G., Zhang, C., and Philip, S. Y. A comprehensive survey on graph neural networks. *TNNLS*, 2020.

Xu, K., Hu, W., Leskovec, J., and Jegelka, S. How powerful are graph neural networks? In *ICLR*, 2019.

You, Y., Chen, T., Sui, Y., Chen, T., Wang, Z., and Shen, Y. Graph contrastive learning with augmentations. In *NeurIPS*, 2020.

Zhang, C., Song, D., Huang, C., Swami, A., and Chawla, N. V. Heterogeneous graph neural network. In *KDD*, 2019.

Zhang, C., Tian, Y., Ju, M., Liu, Z., Ye, Y., Chawla, N., and Zhang, C. Chasing all-round graph representation robustness: Model, training, and optimization. In *ICLR*, 2023.

Zhao, T., Zhang, X., and Wang, S. Graphsmote: Imbalanced node classification on graphs with graph neural networks. In *WSDM*, 2021.

Zhou, D., He, J., Yang, H., and Fan, W. Sparc: Self-paced network representation for few-shot rare category characterization. In *KDD*, 2018.

Zhu, Y., Xu, Y., Yu, F., Liu, Q., Wu, S., and Wang, L. Deep Graph Contrastive Representation Learning. In *ICML Workshop on Graph Representation Learning and Beyond*, 2020.

A. Proof of Theorem 1

We denote the full graph dataset as $\mathcal{D}_F$, the graph data subset used to train the model as $\mathcal{D}_S$, the learning rate as α, and the graph learning model parameters as θ (the optimal model parameters as θ^*). Additionally, we add a superscript to represent the model's parameters and the graph data subset at epoch t, i.e., $\theta^{(t)}$ and $\mathcal{D}_S^{(t)}$. Furthermore, we use $\mathcal{L}_{\mathcal{D}_S^{(t)};\theta^{(t)}}$ to indicate the loss of model $\theta^{(t)}$ over the graph dataset $\mathcal{D}_S^{(t)}$. Thus, the gradient error at training epoch t can be computed as $\mathrm{Err}^{(t)} = \left\| \nabla_{\theta^{(t)}} \mathcal{L}_{\mathcal{D}_S^{(t)};\theta^{(t)}} - \nabla_{\theta^{(t)}} \mathcal{L}_{\mathcal{D}_F;\theta^{(t)}} \right\|$.

The sparse graph subset approximation hypothesis states that the model effectiveness trained on $\mathcal{D}$ can be approximated by the one trained on $\mathcal{D}_S$. To establish this, we make the following assumptions:

Assumption 1. *The model's parameters at epoch t satisfies $\left\|\theta^{(t)}\right\|^2 \leqslant d^2$, where d is a constant.*

Assumption 2. *The loss function $\mathcal{L}(\cdot)$ is convex.*

These assumptions align with previous theoretical papers on GNNs (Chen et al., 2023) or on the subset training of general machine learning (Mirzasoleiman et al., 2020; Killamsetty et al., 2021), which have also followed this philosophy to study the properties of GNNs or analyze subset training in neural networks. Based on these assumptions, we can establish the following theorem:

Theorem 1. *Consider any model and loss function that satisfy Assumption 1 and Assumption 2, respectively. If the training loss $\mathcal{L}_{\mathcal{D}_S}$ is Lipschitz continuous, $\nabla_{\theta^{(t)}} \mathcal{L}_{\mathcal{D}_S}$ is upper-bounded by σ, and $\alpha = \frac{d}{\sigma\sqrt{T}}$, then*

$$\min_t (\mathcal{L}_{\mathcal{D}_F;\theta^{(t)}} - \mathcal{L}_{\theta*}) \leqslant \frac{d\sigma}{\sqrt{T}} + \sum_{t=1}^{T-1} \frac{d}{T} \mathrm{Err}^{(t)}. \tag{9}$$

Proof. The gradients of training loss $\mathcal{L}_{\mathcal{D}_S^{(t)};\theta^{(t)}}$ at epoch t are supposed to be σ-bounded by σ. According to gradient descent, we have:

$$\nabla_\theta \mathcal{L}_{\mathcal{D}_S^{(t)};\theta^{(t)}} (\theta^{(t)})^\top (\theta^{(t)} - \theta^*) = \frac{1}{\alpha^{(t)}} (\theta^{(t)} - \theta^{(t+1)})^\top (\theta^{(t)} - \theta^*), \tag{10}$$

which can be rewritten as:

$$\nabla_\theta \mathcal{L}_{\mathcal{D}_S^{(t)};\theta^{(t)}} (\theta^{(t)})^\top (\theta^{(t)} - \theta^*) = \frac{1}{2\alpha^{(t)}} \left(\left\|\theta^{(t)} - \theta^{(t+1)}\right\|^2 + \left\|\theta^{(t)} - \theta^*\right\|^2 - \left\|\theta^{(t+1)} - \theta^*\right\|^2 \right). \tag{11}$$

Since one update step $\theta^{(t)} - \theta^{(t+1)}$ can be optimized by gradient multiplying with learning rate $\alpha^{(t)} \nabla_\theta \mathcal{L}_{\mathcal{D}_S^{(t)};\theta^{(t)}} (\theta^{(t)})$, we have:

$$\nabla_\theta \mathcal{L}_{\mathcal{D}_S^{(t)};\theta^{(t)}} (\theta^{(t)})^\top (\theta^{(t)} - \theta^*) = \frac{1}{2\alpha^{(t)}} \left(\left\|\alpha^{(t)} \nabla_\theta \mathcal{L}_{\mathcal{D}_S^{(t)};\theta^{(t)}} (\theta^{(t)})\right\|^2 + \left\|\theta^{(t)} - \theta^*\right\|^2 - \left\|\theta^{(t+1)} - \theta^*\right\|^2 \right). \tag{12}$$

Combining this with:

$$\begin{aligned} \nabla_\theta \mathcal{L}_{\mathcal{D}_S^{(t)};\theta^{(t)}} (\theta^{(t)})^\top (\theta^{(t)} - \theta^*) &= \nabla_\theta \mathcal{L}_{\mathcal{D}_S^{(t)};\theta^{(t)}} (\theta^{(t)})^\top (\theta^{(t)} - \theta^*) \\ &- \nabla_\theta \mathcal{L}_{\mathcal{D}_F;\theta^{(t)}}{}^\top (\theta^{(t)} - \theta^*) + \nabla_\theta \mathcal{L}_{\mathcal{D}_F;\theta^{(t)}}{}^\top (\theta^{(t)} - \theta^*), \end{aligned} \tag{13}$$

we obtain:

$$\begin{aligned} &\nabla_\theta \mathcal{L}_{\mathcal{D}_S^{(t)};\theta^{(t)}} (\theta^{(t)})^\top (\theta^{(t)} - \theta^*) - \nabla_\theta \mathcal{L}_{\mathcal{D}_F;\theta^{(t)}}{}^\top (\theta^{(t)} - \theta^*) + \nabla_\theta \mathcal{L}_{\mathcal{D}_F;\theta^{(t)}}{}^\top (\theta^{(t)} - \theta^*) = \\ &\qquad \frac{1}{2\alpha^{(t)}} \left(\left\|\alpha^{(t)} \nabla_\theta \mathcal{L}_{\mathcal{D}_S^{(t)};\theta^{(t)}} (\theta^{(t)})\right\|^2 + \left\|\theta^{(t)} - \theta^*\right\|^2 - \left\|\theta^{(t+1)} - \theta^*\right\|^2 \right) \end{aligned} \tag{14}$$

$$\begin{aligned} \nabla_\theta \mathcal{L}_{\mathcal{D}_F;\theta^{(t)}}{}^\top (\theta^{(t)} - \theta^*) = \frac{1}{2\alpha^{(t)}} &\left(\left\|\alpha^{(t)} \nabla_\theta \mathcal{L}_{\mathcal{D}_S^{(t)};\theta^{(t)}} (\theta^{(t)})\right\|^2 + \left\|\theta^{(t)} - \theta^*\right\|^2 - \left\|\theta^{(t+1)} - \theta^*\right\|^2 \right) \\ &- \left(\nabla_\theta \mathcal{L}_{\mathcal{D}_S^{(t)};\theta^{(t)}} (\theta^{(t)}) - \nabla_\theta \mathcal{L}_{\mathcal{D}_F;\theta^{(t)}} \right)^\top (\theta^{(t)} - \theta^*). \end{aligned} \tag{15}$$

Assuming the learning rate $\alpha^{(t)}, t \in [0, T-1]$ is a constant value α, we can simplify this to:

$$\sum_{t=0}^{T-1} \nabla_\theta \mathcal{L}_{\mathcal{D}_F;\theta^{(t)}}{}^\top (\theta^{(t)} - \theta^*) = \frac{1}{2\alpha}\left\|\theta^{(0)} - \theta^*\right\|^2 - \frac{1}{2\alpha}\left\|\theta^{(t)} - \theta^*\right\|^2 + \sum_{t=0}^{T-1}\left(\frac{1}{2\alpha}\left\|\alpha \nabla_\theta \mathcal{L}_{\mathcal{D}_S^{(t)};\theta^{(t)}}(\theta^{(t)})\right\|^2\right) + \sum_{t=0}^{T-1}\left(\left(\nabla_\theta \mathcal{L}_{\mathcal{D}_S^{(t)};\theta^{(t)}}(\theta^{(t)}) - \nabla_\theta \mathcal{L}_{\mathcal{D}_F;\theta^{(t)}}\right)^\top (\theta^{(t)} - \theta^*)\right).$$

Considering that $\left\|\theta^{(t)} - \theta^*\right\|^2 \geqslant 0$, we can simplify further:

$$\begin{aligned}\sum_{t=0}^{T-1} \nabla_\theta \mathcal{L}_{\mathcal{D}_F;\theta^{(t)}}{}^\top (\theta^{(t)} - \theta^*) \leqslant \frac{1}{2\alpha}\left\|\theta^{(0)} - \theta^*\right\|^2 + \sum_{t=0}^{T-1}\left(\frac{1}{2\alpha}\left\|\alpha \nabla_\theta \mathcal{L}_{\mathcal{D}_S^{(t)};\theta^{(t)}}(\theta^{(t)})\right\|^2\right) \\ + \sum_{t=0}^{T-1}\left(\left(\nabla_\theta \mathcal{L}_{\mathcal{D}_S^{(t)};\theta^{(t)}}(\theta^{(t)}) - \nabla_\theta \mathcal{L}_{\mathcal{D}_F;\theta^{(t)}}\right)^\top (\theta^{(t)} - \theta^*)\right).\end{aligned} \tag{16}$$

Assuming the loss $\mathcal{L}$ is convex and the training loss $\mathcal{L}_{\mathcal{D}_S^{(t)};\theta^{(t)}}$ is Lipschitz continuous with parameter σ, we have $\mathcal{L}_{\mathcal{D}_S^{(t)};\theta^{(t)}} - \mathcal{L}_{\theta*} \leqslant \nabla_\theta \mathcal{L}_{\mathcal{D}_S^{(t)};\theta^{(t)}}{}^\top (\theta^{(t)} - \theta^*)$. Combining this with the previous inequality, we obtain:

$$\begin{aligned}\sum_{t=0}^{T-1} \nabla_\theta \mathcal{L}_{\mathcal{D}_F;\theta^{(t)}} - \mathcal{L}_{\theta*} \leqslant \frac{1}{2\alpha}\left\|\theta^{(0)} - \theta^*\right\|^2 + \sum_{t=0}^{T-1}\left(\frac{1}{2\alpha}\left\|\alpha \nabla_\theta \mathcal{L}_{\mathcal{D}_S^{(t)};\theta^{(t)}}(\theta^{(t)})\right\|^2\right) \\ + \sum_{t=0}^{T-1}\left(\left(\nabla_\theta \mathcal{L}_{\mathcal{D}_S^{(t)};\theta^{(t)}}(\theta^{(t)}) - \nabla_\theta \mathcal{L}_{\mathcal{D}_F;\theta^{(t)}}\right)^\top (\theta^{(t)} - \theta^*)\right).\end{aligned} \tag{17}$$

Since $\left\|\mathcal{L}_{\mathcal{D}_S^{(t)};\theta^{(t)}}(\theta)\right\| \leqslant \sigma$, $\left\|\alpha \nabla_\theta \mathcal{L}_{\mathcal{D}_S^{(t)};\theta^{(t)}}(\theta^{(t)})\right\| \leqslant \sigma$, and we assume $\|\theta - \theta^*\| \leqslant \sqrt{2}d$ (based on Assumption 1), we have:

$$\sum_{t=0}^{T-1} \mathcal{L}_{\mathcal{D}_F;\theta^{(t)}} - \mathcal{L}_{\theta*} \leqslant \frac{d^2}{2\alpha} + \frac{T\alpha\sigma^2}{2} + \sum_{t=0}^{T-1} d\left(\left\|\nabla_\theta \mathcal{L}_{\mathcal{D}_S^{(t)};\theta^{(t)}}(\theta^{(t)}) - \nabla_\theta \mathcal{L}_{\mathcal{D}_F;\theta^{(t)}}\right\|\right), \tag{18}$$

Dividing both sides of the inequality by T gives:

$$\frac{1}{T}\sum_{t=0}^{T-1} \mathcal{L}_{\mathcal{D}_F;\theta^{(t)}} - \mathcal{L}_{\theta*} \leqslant \frac{d^2}{2\alpha T} + \frac{\alpha\sigma^2}{2} + \sum_{t=0}^{T-1} \frac{d}{T}\left(\left\|\nabla_\theta \mathcal{L}_{\mathcal{D}_S^{(t)};\theta^{(t)}}(\theta^{(t)}) - \nabla_\theta \mathcal{L}_{\mathcal{D}_F;\theta^{(t)}}\right\|\right). \tag{19}$$

Since $\min\left(\mathcal{L}_{\mathcal{D}_F;\theta^{(t)}} - \mathcal{L}_{\theta*}\right) \leqslant \frac{1}{T}\sum_{t=0}^{T-1} \mathcal{L}_{\mathcal{D}_S^{(t)};\theta^{(t)}} - \mathcal{L}_{\theta*}$, based on Equation 19, we have:

$$\min\left(\mathcal{L}_{\mathcal{D}_F;\theta^{(t)}} - \mathcal{L}_{\theta*}\right) \leqslant \frac{d^2}{2\alpha T} + \frac{\alpha\sigma^2}{2} + \sum_{t=0}^{T-1} \frac{d}{T}\left(\left\|\nabla_\theta \mathcal{L}_{\mathcal{D}_S^{(t)};\theta^{(t)}}(\theta^{(t)}) - \nabla_\theta \mathcal{L}_{\mathcal{D}_F;\theta^{(t)}}\right\|\right). \tag{20}$$

Finally, by setting the learning rate $\alpha = \frac{d}{\sigma\sqrt{T}}$ and simplifying, we arrive at the desired result:

$$\min\left(\mathcal{L}_{\mathcal{D}_F;\theta^{(t)}} - \mathcal{L}_{\theta*}\right) \leqslant \frac{d\sigma}{\sqrt{T}} + \sum_{t=0}^{T-1} \frac{d}{T}\left(\left\|\nabla_\theta \mathcal{L}_{\mathcal{D}_S^{(t)};\theta^{(t)}}(\theta^{(t)}) - \nabla_\theta \mathcal{L}_{\mathcal{D}_F;\theta^{(t)}}\right\|\right). \tag{21}$$

This completes the proof of Theorem 1. □

B. Preliminaries: GNNs, Graph Contrastive Learning, Network Pruning

In this work, we denote graph as $G = (V, E, X)$, where V is the set of nodes, E is the set of edges, and $X \in \mathbb{R}^d$ represents the node (and edge) attributes of dimension d. In addition, we represent the neighbor set of node $v \in V$ as N_v.

Graph Neural Networks. GNNs (Wu et al., 2020) learn node representations from the graph structure and node attributes. This process can be formulated as:

$$h_v^{(l)} = \text{COMBINE}^{(l)}\left(h_v^{(l-1)}, \text{AGGREGATE}^{(l)}\left(\left\{h_u^{(l-1)}, \forall u \in N_v\right\}\right)\right), \tag{22}$$

where $h_v^{(l)}$ denotes representation of node v at l-th GNN layer; $\text{AGGREGATE}(\cdot)$ and $\text{COMBINE}(\cdot)$ are neighbor aggregation and combination functions, respectively; $h_v^{(0)}$ is initialized with node attribute X_v. We obtain the output representation of each node after repeating the process in Equation (22) for L rounds. The representation of the whole graph, denoted as $h_G \in \mathbb{R}^d$, can be obtained by using a READOUT function to combine the final node representations learned above:

$$h_G = \text{READOUT}\left\{h_v^{(L)} \mid \forall v \in V\right\}, \tag{23}$$

where the READOUT function can be any permutation invariant, like summation, averaging, etc.

Graph Contrastive Learning. Given a graph dataset $\mathcal{D} = \{G_i\}_{i=1}^N$, Graph Contrastive Learning (GCL) methods firstly implement proper transformations on each graph G_i to generate two views G_i' and G_i''. The goal of GCL is to map samples within positive pairs closer in the hidden space, while those of the negative pairs are further. GCL methods are usually optimized by a contrastive loss. Taking the most popular InfoNCE loss (Oord et al., 2018) as an example, the contrastive loss is defined as:

$$\mathcal{L}_{CL}(G_i', G_i'') = -\log \frac{\exp\left(\text{sim}\left(\mathbf{z}_{i,1}, \mathbf{z}_{i,2}\right)\right)}{\sum_{j=1, j\neq i}^{N} \exp\left(\text{sim}\left(\mathbf{z}_{i,1}, \mathbf{z}_{j,2}\right)\right)}, \tag{24}$$

where $\mathbf{z}_{i,1} = f_\theta\left(G_i'\right)$, $\mathbf{z}_{i,2} = f_\theta\left(G_i''\right)$, and sim denotes the similarity function.

Network Pruning. Given an over-parameterized deep neural network $f_\theta(\cdot)$ with weights θ, the network pruning is usually performed layer-by-layer. The pruning process of the l_{th} layer in $f_\theta(\cdot)$ can be formulated as follows:

$$\theta_{pruned}^{l_{th}} = \text{TopK}(\theta^{l_{th}}, k), k = \alpha \times |\theta^{l_{th}}|, \tag{25}$$

where $\theta^{l_{th}}$ is the parameters in the l_{th} layer of $f_\theta(\cdot)$ and $\text{TopK}(\cdot, k)$ refers to the operation to choose the top-k largest elements of $\theta^{l_{th}}$. We use a pre-defined sparse rate α to control the fraction of parameters kept in the pruned network $\theta_{pruned}^{l_{th}}$. Finally, only the top $k = \alpha \times |\theta^{l_{th}}|$ largest weights will be kept in the pruned layer. The pruning process will be implemented iteratively to prune the parameters in each layer of deep neural network (Han et al., 2015a).

C. Experimental Details

C.1. Datasets Details

In this work, seven graph classification datasets and five node classification datasets are used to evaluate the effectiveness of our proposed model, we provided their detailed statistics in Table 5. For graph classification datasets, we follow the imbalance setting of (Wang et al., 2022) to set the train-validation split as 25%/25% and change the imbalance ratio from 5:5 (balanced) to 1:9 (imbalanced). The rest of the dataset is used as the test set. The specified imbalance ratio of each dataset is clarified after its name in Table 6. For node classification datasets, we follow (Sen et al., 2008) to set the imbalance ratio of Cora, CiteSeer and PubMed as 10. Besides, the setting of Amazon-Photo and Amazon-Computers are borrowed from (Park et al., 2022), where the imbalance ratio ρ is set as 82 and 244, respectively.

C.2. Baseline Details

We compare our model with a variety of baseline methods using different rebalance methods:

I. For **imbalanced graph classification** (Wang et al., 2022), four models are included as baselines in our work, we list these baselines as follow:

(1) **GIN** (Xu et al., 2019), a popular supervised GNN backbone for graph tasks due to its powerful expressiveness on graph structure;

(2) **InfoGraph** (Sun et al., 2019), an unsupervised graph learning framework by maximizing the mutual information between the whole graph and its local topology of different levels;

Table 5: Original dataset details for imbalanced graph classification and imbalanced node classification tasks.

Task	Dataset	# Graphs	# Nodes	# Edges	# Features	# Classes
Graph	MUTAG	188	~17.93	~19.79	-	2
	PROTEINS	1,113	~39.06	~72.82	-	2
	D&D	1,178	~284.32	~715.66	-	2
	NCI1	4,110	~29.87	~32.30	-	2
	PTC-MR	344	~14.29	~14.69	-	2
	DHFR	756	~42.43	~44.54	-	2
	REDDIT-B	2,000	~429.63	~497.75	-	2
Node	Cora	-	2,485	5,069	1,433	7
	Citeseer	-	2,110	3,668	3,703	6
	Pubmed	-	19,717	44,324	500	3
	A-photo	-	7,650	238,162	745	8
	A-computers	-	13,381	245,778	767	10

(3) **GraphCL** (You et al., 2020), learning unsupervised graph representations via maximizing the mutual information between the original graph and corresponding augmented views;

(4) **G^{2}GNN** (Wang et al., 2022), a re-balanced GNN proposed to utilize additional supervisory signals from both neighboring graphs and graphs themselves to alleviate the imbalance issue of graph.

II. For **imbalanced node classification**, we consider nine baseline methods in our work, including

(1) **vanilla**, denoting that we train GCN normally without any extra rebalancing tricks;

(2) **re-weight** (Japkowicz & Stephen, 2002), denoting we use cost-sensitive loss and re-weight the penalty of nodes in different classes;

(3) **oversampling** (Park et al., 2022), denoting that we sample nodes of each class to make the data's number of each class reach the maximum number of corresponding class's data;

(4) **cRT** (Kang et al., 2020), a post-hoc correction method for decoupling output representations;

(5) **PC Softmax** (Hong et al., 2021), a post-hoc correction method for decoupling output representations, too;

(6) **DR-GCN** (Shi et al., 2020), building virtual minority nodes and forces their features to be close to the neighbors of a source minority node;

(7) **GraphSMOTE** (Zhao et al., 2021), a pre-processing method that focuses on the input data and investigates the possibility of re-creating new nodes with minority features to balance the training data.

(8) **GraphENS** (Park et al., 2022), proposing a new augmentation method to construct an ego network from all nodes for learning minority representation.

(9) **SynFlow** (Tanaka et al., 2020), a one-shot model pruning method with less reliance on data.

(10) **BGRL** (Thakoor et al., 2021), a graph contrastive learning method using only simple augmentations and avoids the requirements for contrasting with negative examples, and thus makes itself scalable.

(11) **GRACE** (Zhu et al., 2020), a graph contrastive learning method generating two views by corrupting a graph and learning node embeddings by minimizing the distance of node embeddings in these two views.

We use Graph Convolutional Network (GCN) (Kipf & Welling, 2017) as the default architecture for all rebalance methods.

C.3. Details of DataDec Variants

The details of model variants are provided as follows:

I. Specifically, DataDec contains four components to address data sparsity and imbalance: (1) **GS** is sampling informative

Table 6: Class-imbalanced graph classification results. The numbers after each dataset name indicate the imbalance ratios of minority to majority categories. We report the macro F1-score and micro F1-score with the standard errors as Results are reported as $mean \pm std$ for 3 repetitions on each dataset. We bold the best performance.

Rebalance Method	Basis	MUTAG (5:45)		PROTEINS (30:270)		D&D (30:270)		NCI1 (100:900)	
		F1-ma.	F1-mi.	F1-ma.	F1-mi.	F1-ma.	F1-mi.	F1-ma.	F1-mi.
vanilla	GIN (Xu et al., 2019)	52.50 ± 18.70	56.77 ± 14.14	25.33 ± 7.53	28.50 ± 5.82	9.99 ± 7.44	11.88 ± 9.49	18.24 ± 7.58	18.94 ± 7.12
	InfoGraph (Sun et al., 2019)	69.11 ± 9.03	69.68 ± 7.77	35.91 ± 7.58	36.81 ± 6.51	21.41 ± 4.51	27.68 ± 7.52	33.09 ± 3.30	34.03 ± 3.68
	GraphCL (You et al., 2020)	66.82 ± 11.56	67.77 ± 9.78	40.86 ± 6.94	41.24 ± 6.38	21.02 ± 3.05	26.80 ± 4.95	31.02 ± 2.69	31.62 ± 3.05
up-sampling	GIN (Xu et al., 2019)	78.03 ± 7.62	78.77 ± 7.67	65.64 ± 2.67	71.55 ± 3.19	41.15 ± 3.74	70.56 ± 10.28	59.19 ± 4.39	71.80 ± 7.02
	InfoGraph (Sun et al., 2019)	78.62 ± 6.84	79.09 ± 6.86	62.68 ± 2.70	66.02 ± 3.18	41.55 ± 2.32	71.34 ± 6.76	53.38 ± 1.88	62.20 ± 2.63
	GraphCL (You et al., 2020)	80.06 ± 7.79	80.45 ± 7.86	64.21 ± 2.53	65.76 ± 2.61	38.96 ± 3.01	64.23 ± 8.10	49.92 ± 2.15	58.29 ± 3.30
re-weight	GIN (Xu et al., 2019)	77.00 ± 9.59	77.68 ± 9.30	54.54 ± 6.29	55.77 ± 7.11	28.49 ± 5.92	40.79 ± 11.84	36.84 ± 8.46	39.19 ± 10.05
	InfoGraph (Sun et al., 2019)	80.85 ± 7.75	81.68 ± 7.83	65.73 ± 3.10	69.60 ± 3.68	41.92 ± 2.28	72.43 ± 6.63	53.05 ± 1.12	62.45 ± 1.89
	GraphCL (You et al., 2020)	80.20 ± 7.27	80.84 ± 7.43	63.46 ± 2.42	64.97 ± 2.41	40.29 ± 3.31	67.96 ± 8.98	50.05 ± 2.09	58.18 ± 3.08
G^2GNN (Wang et al., 2022)	remove edge	80.37 ± 6.73	81.25 ± 6.87	67.70 ± 2.96	73.10 ± 4.05	43.25 ± 3.91	77.03 ± 9.98	63.60 ± 1.57	72.97 ± 1.81
	mask node	83.01 ± 7.01	83.59 ± 7.14	67.39 ± 2.99	73.30 ± 4.19	43.93 ± 3.46	79.03 ± 10.78	64.78 ± 2.86	74.91 ± 2.14
DataDec	dynamic sparsity	**85.71±10.20**	**85.71±11.10**	**68.31±4.23**	**75.84±6.80**	**44.01±5.01**	77.02 ± 6.26	**65.73±4.7**	**76.02±6.27**

Rebalance Method	Basis	PTC-MR (9:81)		DHFR (12:108)		REDDIT-B (50:450)	
		F1-ma.	F1-mi.	F1-ma.	F1-mi.	F1-ma.	F1-mi.
vanilla	GIN (Xu et al., 2019)	17.74 ± 6.49	20.30 ± 6.06	35.96 ± 8.87	49.46 ± 4.90	33.19 ± 14.26	36.02 ± 17.38
	InfoGraph (Sun et al., 2019)	25.85 ± 6.14	26.71 ± 6.50	50.62 ± 8.33	56.28 ± 4.58	57.67 ± 3.80	67.10 ± 4.91
	GraphCL (You et al., 2020)	24.22 ± 6.21	25.16 ± 5.25	50.55 ± 10.01	56.31 ± 6.12	53.40 ± 4.06	62.19 ± 5.68
up-sampling	GIN (Xu et al., 2019)	44.78 ± 8.01	55.43 ± 14.25	55.96 ± 10.06	59.39 ± 6.52	66.71 ± 3.92	83.00 ± 5.18
	InfoGraph (Sun et al., 2019)	44.29 ± 4.69	48.91 ± 7.49	59.49 ± 5.20	61.62 ± 4.18	67.01 ± 3.34	78.68 ± 3.71
	GraphCL (You et al., 2020)	45.12 ± 7.33	53.50 ± 13.31	60.29 ± 9.04	61.71 ± 6.75	62.01 ± 3.97	75.84 ± 3.98
re-weight	GIN (Xu et al., 2019)	36.96 ± 14.08	43.09 ± 20.01	55.16 ± 9.47	57.78 ± 6.69	45.17 ± 8.46	51.92 ± 12.29
	InfoGraph (Sun et al., 2019)	44.09 ± 5.62	49.17 ± 8.78	58.67 ± 5.82	60.24 ± 4.80	65.79 ± 3.38	77.35 ± 3.96
	GraphCL (You et al., 2020)	44.75 ± 7.62	52.22 ± 13.24	60.87 ± 6.33	61.93 ± 5.15	62.79 ± 6.93	76.15 ± 9.15
G^2GNN (Wang et al., 2022)	remove edge	46.40 ± 7.73	56.61 ± 13.72	61.63 ± 10.02	63.61 ± 6.05	68.39 ± 2.97	86.35 ± 2.27
	mask node	46.61 ± 8.27	56.70 ± 14.81	59.72 ± 6.83	61.27 ± 5.40	67.52 ± 2.60	85.43 ± 1.80
DataDec	dynamic sparsity	**47.07±8.22**	**58.15±10.24**	**62.25±9.54**	**63.61±7.10**	**69.70±7.20**	**87.00±9.36**

subset data according to ranking gradients; (2) **SS** is training model with the sparse dataset, correspondingly; (3) **CAD** is using cosine annealing to reduce dataset size; (4) **RS** is recycling removed samples, correspondingly. To investigate their corresponding effectiveness, we remove them correspondingly as:

(1) **w/o GS** is that we randomly sample subset from the full set;

(2) **w/o SS** is that we train GNN with the full set;

(3) **w/o CAD** is that we directly reduce dataset size to target dataset size and it is same as data diet;

(4) **w/o RS** is not recycling any removed samples.

II. Another four components to address model sparsity and data imbalance: (1) **RM** samples model weights according to ranking magnitudes; (2) **SG** is using sparse GNN, correspondingly; (3) **CAG** is using cosine annealing to progressively reduce sparse GNN's size; (4) **RW** is reactivating removed weights. To investigate their effectiveness, we remove them correspondingly as:

(1) **w/o RM** is that we randomly sample activated weights from full GNN model;

(2) **w/o SG** is that we train full GNN during forward and backward;

(3) **w/o CAG** is that we directly reduce the model size to target sparsity rate;

(4) **w/o RW** is not reactivating any removed weights during sparse training.

C.4. Full Results with Error Bars

We provide the F1-macro and F1-micro scores along with their standard deviation for our model and other baselines across both graph classification and node classification tasks in Table 6 and Table 7. We report their results as $mean \pm std$ for 3 repetitions on each metric for each dataset.

Table 7: Class-imbalanced node classification results. We report the accuracy, balanced accuracy, and macro F1-score with the standard errors as $mean \pm std$ for 3 repetitions on each dataset. We bold the best performance.

Method	Cora-LT			CiteSeer-LT			PubMed-LT			A.P. (ρ =82)		A.C. (ρ =244)	
	Acc.	bAcc.	F1-ma.	Acc.	bAcc.	F1-ma.	Acc.	bAcc.	F1-ma.	(b)Acc.	F1-ma.	(b)Acc.	F1-ma.
vanilla	73.66±0.28	62.72±0.39	63.70±0.43	53.90±0.70	47.32±0.61	43.00±0.70	70.76±0.74	57.56±0.59	51.88±0.53	82.86±0.30	78.72±0.52	68.47±2.19	64.01±3.18
SynFlow (Tanaka et al., 2020)	72.98	60.62	63.29	52.85	46.23	42.19	69.63	56.75	50.99	81.57	76.93	68.10	62.97
GRACE (Zhu et al., 2020)	74.72	63.95	65.26	54.94	50.87	46.90	72.37	63.22	58.18	83.57	83.61	73.02	64.52
BGRL (Thakoor et al., 2021)	73.81	64.95	64.87	56.84	50.83	47.04	74.17	62.21	59.07	83.49	82.37	75.88	63.15
Re-Weight (Park et al., 2022)	75.20±0.19	68.79±0.18	69.27±0.26	62.56±0.32	55.80±0.28	53.74±0.28	77.44±0.21	72.80±0.38	73.66±0.27	92.94±0.13	92.95±0.13	90.04±0.29	90.11±0.28
Oversampling (Park et al., 2022)	77.44±0.09	70.73±0.10	72.40±0.11	62.78±0.37	56.01±0.35	53.99±0.37	76.70±0.48	68.49±0.28	69.50±0.38	92.46±0.47	92.47±0.48	89.79±0.16	89.85±0.17
cRT (Kang et al., 2020)	76.54±0.22	69.26±0.48	70.95±0.50	60.60±0.25	54.05±0.22	52.36±0.22	75.10±0.23	67.52±0.72	68.08±0.85	91.24±0.28	91.17±0.29	86.02±0.55	86.00±0.56
PC Softmax (Hong et al., 2021)	76.42±0.34	71.30±0.45	71.24±0.52	65.70±0.42	61.54±0.45	61.49±0.49	76.92±0.26	75.82±0.25	74.19±0.25	93.32±0.25	93.32±0.25	86.59±0.92	86.62±0.91
DR-GCN (Shi et al., 2020)	73.90±0.29	64.30±0.39	63.10±0.57	56.18±1.10	49.57±1.08	44.98±1.29	72.38±0.19	58.86±0.15	53.05±0.13	N/A	N/A	N/A	N/A
GraphSmote (Zhao et al., 2021)	76.76±0.31	69.31±0.37	70.21±0.64	62.58±0.30	55.94±0.34	54.09±0.37	75.98±0.22	70.96±0.36	71.85±0.32	92.65±0.31	92.61±0.32	89.31±0.34	89.39±0.35
GraphENS (Park et al., 2022)	77.76±0.09	72.94±0.15	73.13±0.11	66.92±0.21	60.19±0.21	58.67±0.25	78.12±0.06	74.13±0.22	74.58±0.13	93.82±0.13	93.81±0.12	91.94±0.17	91.94±0.17
DataDec	**78.29±0.40**	**73.94±0.67**	**74.25±0.83**	**66.90±0.65**	**61.56±0.72**	**61.85±0.96**	**78.20±0.45**	**76.05±0.66**	**76.32±0.66**	**93.85±0.72**	**94.02±0.67**	**92.19±0.73**	**92.16±0.75**

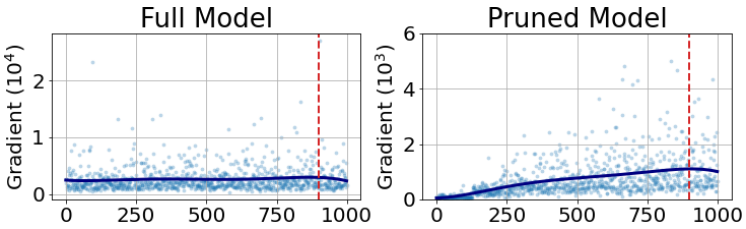

Figure 5: Results of data samples' gradients computed by full GNN model and our dynamic sparse GNN model on NCI1 data. Red dashed line: on the left side, points on the x-axis [0, 900] are majority class; on the right side, points on the x-axis [900, 1000] are minority class.

D. Finding Informative Samples by Sparse GNN

Compared with the full GNN model, our dynamic sparse GNN model is more sensitive in recognizing informative data samples which can be empirically verified by Figure 5. As we can see in the figure, our dynamic pruned model assigns larger gradients to the minorities than the majorities during the contrastive training, while the full model generally assigns relatively uniform gradients for both of them. Thus, the proposed dynamically pruned model demonstrates its discriminatory ability on the minority class.

E. Resource Cost

To evaluate the proposed DataDec's computational cost on a wide range of datasets, results in Table 8 that include three different class-imbalanced node classification datasets (PubMed-LT, Cora-LT, CiteSeer-LT), three different class-imbalanced graph classification datasets (MUTAG, PROTEINS, PTC_MR), and four baselines (vanilla GCN, re-weight, re(/over)-sample, GraphCL). We run 200 epochs for each method to measure their computational time (second) for training. On NVIDIA GeForce RTX 3090 GPU device, we obtain the running time as reported in Table 8. All models are implemented in PyTorch Geometric (Fey & Lenssen, 2019).

Table 8: Computational time comparisons.

Model	Method	PubMed-LT	Cora-LT	CiteSeer-LT	PROTEINS	PTC_MR	MUTAG
GCN	vanilla	2.436	2.154	2.129	12.798	4.295	2.989
	re-weight	2.330	2.282	2.150	12.903	4.410	3.125
	re(/over)-sample	3.241	2.860	2.794	15.996	5.734	4.022
	GraphCL	3.747	3.412	3.399	14.981	5.049	3.215
	DataDec	2.243	1.995	1.952	10.614	4.212	2.090

According to the results, our DataDec encounters less computation cost than prior methods. The following explains why augmentation doubles the input graph without increasing overall computation costs: (i) The augmentations we adopt (e.g, node dropping and edge dropping) reduce the size of input graphs (i.e., node number decreases 25%, edge number decreases 25-35%); (ii) During each epoch, our DataDec prunes datasets so that approximately only 50% of the training data is used. (iii) DataDec prunes the model weights, resulting in a lighter model requiring less computational resources. (iv) Despite the

fact that augmentation doubles the number of input graphs, the additional new views only consume forward computational resources without requiring a backward or weight update step, thereby only marginally increases the computation.